Elliptic Harbor Wave Model with Perfectly Matched Layer and Exterior Bathymetry Effects

David Modesto [1]; Sonia Fernández-Méndez[2]; and Antonio Huerta, P.E., Member ASCE[3]

ABSTRACT

Standard strategies for dealing with the Sommerfeld condition in elliptic Mild-Slope models require strong assumptions on the wave field in the region exterior to the computational domain. More precisely, constant bathymetry along (and beyond) the open boundary, and parabolic-approximations based boundary conditions are usually imposed. In general, these restrictions require large computational domains, implying higher costs for the numerical solver. An alternative method for coastal/harbor applications is proposed here. This approach is based on a Perfectly Matched Layer (PML) that incorporates the effects of the exterior bathymetry. The model only requires constant exterior depth in the alongshore direction, a commonly used approach for idealizing the exterior bathymetry in elliptic models. In opposition to standard open boundary conditions for Mild-Slope models, the features of the proposed PML approach include: (a) completely non-collinear coastlines, (b) better representation of the real unbounded domain using two different lateral sections to define the exterior bathymetry, and (c) generation of reliable solutions for any incoming wave direction in a small computational domain. Numerical results of synthetic tests demonstrate that

[1]Graduate Student, Laboratori de Calcul Numeric (LaCaN), E.T.S. de Ingenieros de Caminos, Canales y Puertos, Universitat Politecnica de Catalunya-BarcelonaTech, Barcelona, Spain. E-mail: david.modesto@upc.edu

[2]Associate Professor, Laboratori de Calcul Numeric (LaCaN), E.T.S. de Ingenieros de Caminos, Canales y Puertos, Universitat Politecnica de Catalunya-BarcelonaTech, Barcelona, Spain. E-mail: sonia.fernandez@upc.edu

[3]Professor, Laboratori de Calcul Numeric (LaCaN), E.T.S. de Ingenieros de Caminos, Canales y Puertos, Universitat Politecnica de Catalunya-BarcelonaTech, Barcelona, Spain. url: www.lacan.upc.edu E-mail: antonio.huerta@upc.edu

solutions are not significantly perturbed when open boundaries are placed close to the area of interest. In more complex problems, this provides important performance improvements in computational time as shown for a real application of harbor agitation.

Keywords: Open boundary, Perfectly Matched Layer, Mild-Slope equation, harbor.

INTRODUCTION

Harbor agitation by gravity waves is commonly predicted using elliptic Mild-Slope models (Berkhoff 1972) in a semi-infinite domain, where the unbounded ocean part is connected to physical boundaries (coastlines or harbor boundaries). Computational cost is compromised by the size of the computational domain, directly related to the location of the artificial or *open boundary*. This location is determined by the inherent hypothesis needed to define the artificial boundary condition imposed and its accuracy. Thus, general and accurate conditions generate smaller domains and provide important computational savings. The goal of this paper is to propose an artificial boundary condition for coastal/harbor applications, capable of reproducing the original semi-infinite solution at a minimum cost for the numerical solver.

Standard strategies prescribing artificial non-reflecting boundary conditions impose an *a priori* knowledge of the solution in the exterior domain. The artificial boundary condition along the open boundary is constructed precisely as a consequence of the imposed solution in the far-field area (e.g. Zubier et al. 2003; Li et al. 2005; Chen et al. 2005; Panchang et al. 2008, among others). However, the exact solution in the outer semi-infinite domain is, in general, not known a priori. Classical models exactly verify the Sommerfeld condition through appropriate Hankel or Green functions (e.g. Tsay and Liu 1983; Xu and Panchang 1993), but for most real problems they are invalid because the classical models require totally reflective and collinear coastlines. Xu et al. (1996) proposed a parabolic-approximation based boundary condition to relax these limitations, but with the downside of not fulfilling exactly the Sommerfeld condition. Moreover, this artificial open boundary requires a constant bathymetry in the exterior domain. This is usually a strong assumption near the

coastline in semi-infinite domains. Panchang et al. (2000) addressed this issue by using an incident wave that includes the exterior refractions provided by a non-constant idealized bathymetry, resulting in important accuracy enhancements. Nevertheless, this strategy is still affected by the parabolic-approximation based boundary condition and its limitations (for instance, dominant radial direction of the scattered wave, and local bathymetry variations that are neglected on the open boundary). As a result, the open boundary requires to be placed far enough from the region of interest, especially for complex shaped harbor problems generating numerous reflections. This implies a larger computational domain and, consequently, higher computational cost.

Here, a different approach overcoming the aforementioned limitations is proposed: the Perfectly Matched Layer (PML) technique, originally proposed by Berenger (1994), is extended for the linear elliptic Mild-Slope including the exterior refractions provided by the actual bathymetry. The PML method can be related to the dissipative *sponge layer* concept applied in a number of coastal models, see for instance Larsen and Dancy 1983; Wei and Kirby 1995; Lee and Yoon 2004; Sharma et al. 2014. The basic idea resides in surrounding the interior domain by an artificial layer that aims to damp the diffracted wave energy of the scattered wave. Both methods (sponge layer and PML) modify the original equations inside the artificial layer. More precisely, the sponge layer method includes a decay reaction term in the original Mild-Slope equation, see Sharma et al. (2014), while the derivatives remain unchanged. Although this can dissipate the diffracted wave energy, it does not ensure a reflectionless interface connecting the interior domain with the artificial layer. As a consequence, spurious reflections may pollute the solution. This issue can be alleviated by enlarging the layer, but also increasing the computational cost.

On the contrary, the PML technique is constructed precisely to be a perfect reflectionless artificial layer independently of the angle of incidence. PML transformation of the Mild-Slope equation also affects the elliptic operator (derivatives), ensuring an analytical continuation of the original solution inside the artificial layer (Teixeira and Chew 2000). Derivation of the

Mild-Slope PML equation following the primary rationale by Berenger (1994) is provided in the Appendix. The PML has been applied in numerous scattering problems in the last decade with excellent performance (e.g. Basu and Chopra 2003; Singer and Turkel 2004; Michler et al. 2007; Demaldent and Imperiale 2013). Unbounded coastal problems with PML and linearized shallow waters equations were addressed by Navon et al. (2004). In harbor agitation with Mild-Slope models, the PML has been also recently used within a model reduction framework by Modesto et al. (2015). These references for coastal modeling are limited by constant exterior bathymetry, and hence no exterior refractions are considered. First PML development with non-constant depth was addressed by Belibassakis et al. (2001), but for complete unbounded domains and simple geometries.

In this paper, a strategy to incorporate the actual bathymetry is formulated for complex harbor problems, using a rectangular shaped PML to approach the real semi-infinite domain. Here, the arbitrary definition of the bathymetry prevents an analytical continuation of the solution in the PML, see Oskooi et al. (2008). In the aim of preserving the PML reflectionless properties, some simplifications on the non-constant far-field bathymetry are imposed. More precisely, this paper uses the idealization of the real water depth suggested by Panchang et al. (2000), representing a good compromise between harbor models and reality. Two different lateral sections of the idealized bathymetry are used, in order to retain the exact water depth in the entire interior domain, and compute the incident wave. Moreover, the proposed PML circumvents the difficulties associated to boundary conditions that apply directly on semicircular artificial boundaries. For instance, it offers the possibility to incorporate fully non-collinear coastlines in a natural manner. Furthermore, it avoids the need of interpolating the incident wave on the open boundary when two sections of the exterior bathymetry are used (e.g. see Zhao et al. 2001). This results in satisfactory approximations of the solution using very reduced computational domains, and for complex geometries that generate numerous reflections.

The PML model is tested with four examples. Scattering on a circular object with

constant bathymetry is solved first to demonstrate the capabilities of the PML for very close open boundaries. A semicircular geometry with variable bathymetry is then used to verify that the idealized semi-infinite domain is properly reproduced. Validation through the standard elliptic shoal test for the Mild-Slope equation has been also addressed (briefly commented in the application section). Finally, to reinforce the validity of the model solution, an application to a real harbor located in the Northeast of Spain is shown.

ELLIPTIC HARBOR MODELS

In linear wave theory, the wave potential or complex surface elevation $\phi(x, y) \in \mathbb{C}$ propagates over the semi-infinite domain $\Omega_\infty \subset \mathbb{R}^2$ by means of the Mild-Slope equation

$$\boldsymbol{\nabla} \cdot (c\, c_g \boldsymbol{\nabla} \phi) + k^2 c\, c_g \phi = 0 \quad \text{in } \Omega_\infty, \tag{1}$$

where $k(x, y) \in \mathbb{R}$ is the wavenumber, $c = \omega/k \in \mathbb{R}$ is the phase velocity, $\omega \in \mathbb{R}$ is the angular frequency of the monochromatic incident wave and $c_g \in \mathbb{R}$ is the group velocity. The wavenumber is related to frequency and to the slow varying bathymetry (i.e. mean-water-level-depth) $h(x, y) \in \mathbb{R}$ to account for refraction effects through the dispersion relation

$$\omega^2 = kg \tanh(kh). \tag{2}$$

The group velocity is then defined as $c_g = d\omega/dk = g[\tanh(kh) + kh\,\mathrm{sech}^2(kh)]/(2\omega)$, with g the acceleration of gravity. Both Eqs. (1) and (2) can be properly modified to incorporate high bathymetry gradients and nonlinear effects, such as wave breaking or bottom friction (e.g. Booij 1981; Kirby 1984; Massel 1993).

This model requires boundary conditions everywhere on the boundary of the semi-infinite domain. Along coastlines and structures (breakwaters, walls, etc.) conforming the physical boundary, namely $\Gamma_{\mathtt{R}}$, the condition is given by Tsay and Liu (1983) as

$$\boldsymbol{n} \cdot c\, c_g \boldsymbol{\nabla} \phi - ikc\, c_g \alpha\, \phi = 0 \quad \text{on } \Gamma_{\mathtt{R}}, \tag{3}$$

where $i = \sqrt{-1}$ is the imaginary unit, $\boldsymbol{n}$ is the outer unit normal at the boundary, and $\alpha \in [0, 1]$ is a real experimental coefficient controlling the reflection/absorption properties of the boundary. This coefficient is equal to zero on perfectly reflecting boundaries and to one on totally absorbing boundaries.

In addition, unbounded scattering problems require the Sommerfeld radiation condition that imposes that the scattered wave only has geometrical diffusion, namely

$$\lim_{r\to\infty} \sqrt{r}\Big(\frac{\partial}{\partial r} - ik\Big)(\phi - \phi_0) = 0, \tag{4}$$

where r is the radial direction and $\phi_0(x, y) \in \mathbb{C}$ the imposed incident wave. Thus, $\phi - \phi_0$ is the scattered wave.

As commented before, Eq. (4) requires a special treatment in order to use a bounded computational domain and reproduce, on the artificial boundary, the effect of the Sommerfeld condition. The PML technique described next is a reasonable alternative in this case.

THE PML MODEL

It is standard practice to truncate the semi-infinite domain, Ω_∞, into an interior region that includes the harbor/areas of interest, $\Omega_{\texttt{int}}$, and a surrounding finite absorbing layer, $\Omega_{\texttt{pml}}$. Thus, the computational domain, Ω, is the union $\overline{\Omega} = \overline{\Omega}_{\texttt{int}} \cup \overline{\Omega}_{\texttt{pml}}$, such that $\Omega \subset \Omega_\infty$.

The PML region is composed of four subdomains as shown in Figure 1, namely $\Omega_{\texttt{pml}} = \Omega^{\texttt{L}x}_{\texttt{pml}} \cup \Omega^{\texttt{R}x}_{\texttt{pml}} \cup \Omega^{y}_{\texttt{pml}} \cup \Omega^{x,y}_{\texttt{pml}}$. This PML is a rectangular shaped layer designed to absorb the scattered wave, along the Cartesian directions x and y, independently of its propagation angle.

The exterior bathymetry in both PML regions $\Omega^{L_x}_{\texttt{pml}}$ and $\Omega^{R_x}_{\texttt{pml}}$ is simplified accordingly to

the usual assumption for harbor models introduced by Panchang et al. (2000),

$$h(x,y) = \begin{cases} h^{\mathtt{L}}(y) & \text{if } (x,y) \in \Omega^{\mathtt{L}x}_{\mathtt{pml}}, \\ h^{\mathtt{R}}(y) & \text{if } (x,y) \in \Omega^{\mathtt{R}x}_{\mathtt{pml}}, \\ h_0 & \text{if } (x,y) \in \Omega^{y}_{\mathtt{pml}} \cup \Omega^{x,y}_{\mathtt{pml}}. \end{cases} \tag{5}$$

This imposes an exterior bathymetry that varies only along the cross-shore direction as shown in Figure 1. The constant value h_0 corresponds to the far-field bathymetry region of the model. It determines the location of the PML at the top part of the computational domain. The exterior coastlines are modeled in the standard way, with straight lines parallel to the x axis, although the PML technique can be generally applied to arbitrary convex domains, see an example by Demaldent and Imperiale (2013). It is important to note that both non-constant exterior bathymetries, $h^{\mathtt{L}}(y)$ and $h^{\mathtt{R}}(y)$, are in general different in order to provide more faithful approximations of the unbounded domain. Moreover, the exterior coastlines have no collinearity assumptions in the present model, i.e. the coordinate $y_c^{\mathtt{L}}$ can be different from $y_c^{\mathtt{R}}$ as shown in Figure 1.

Under these assumptions, the mild-slope PML model reads

$$\boldsymbol{\nabla}\cdot(c\,c_g\mathbf{P}\boldsymbol{\nabla}\phi) + k^2 c\,c_g s_x s_y \phi = f(x,y) \qquad \text{in } \Omega, \tag{6a}$$

$$\boldsymbol{n}\cdot(c\,c_g\mathbf{P}\boldsymbol{\nabla}\phi) - ikc\,c_g\alpha\,\phi = 0 \qquad \text{on } \Gamma_{\mathtt{R}}, \tag{6b}$$

$$\boldsymbol{n}\cdot(c\,c_g\mathbf{P}\boldsymbol{\nabla}\phi) - ikc\,c_g\phi = \boldsymbol{n}\cdot(c\,c_g\mathbf{P}\boldsymbol{\nabla}\phi_0) - ikc\,c_g\phi_0 \qquad \text{on } \Gamma_{\mathtt{pml}}, \tag{6c}$$

where $\partial\Omega = \overline{\Gamma}_{\mathtt{R}} \cup \overline{\Gamma}_{\mathtt{pml}}$. Note that no Dirichlet boundary conditions are imposed. The non-homogeneous source term in (6a) is defined as

$$f = \begin{cases} 0 & \text{if } (x,y) \in \Omega_{\mathtt{int}}, \\ \boldsymbol{\nabla}\cdot(c\,c_g\mathbf{P}\,\boldsymbol{\nabla}\phi_0) + k^2 c\,c_g s_x s_y \phi_0 & \text{if } (x,y) \in \Omega_{\mathtt{pml}}, \end{cases} \tag{7}$$

to account for the incident wave and to absorb only the scattered waves in the PML region. The diagonal anisotropy matrix $\mathbf{P}$ defines the absorption in the PML area and it is the identity matrix in $\Omega_{\mathtt{int}}$, namely

$$\mathbf{P} = \begin{pmatrix} s_y/s_x & 0 \\ 0 & s_x/s_y \end{pmatrix},$$

where $s_x = 1 + i\sigma_x/\omega$ and $s_y = 1 + i\sigma_y/\omega$ are two complex absorption parameters. The usual choice for the functions $\sigma_x(x)$ and $\sigma_y(y)$ are monotonic polynomials in the two respective Cartesian directions, namely

$$\sigma_x(x) = \begin{cases} \sigma_0(|x - x_0|)^n / L_{\mathtt{pml}} & \text{in } \Omega^{\mathtt{L}x}_{\mathtt{pml}} \cup \Omega^{\mathtt{R}x}_{\mathtt{pml}} \cup \Omega^{x,y}_{\mathtt{pml}}, \\ 0 & \text{otherwise}, \end{cases} \tag{8a}$$

$$\sigma_y(y) = \begin{cases} \sigma_0(y - y_0)^n / L_{\mathtt{pml}} & \text{in } \Omega^{y}_{\mathtt{pml}} \cup \Omega^{x,y}_{\mathtt{pml}}, \\ 0 & \text{otherwise}, \end{cases} \tag{8b}$$

where the PML parameters are: σ_0, absorption degree n and PML thickness $L_{\mathtt{pml}}$. The interface $\Omega_{\mathtt{int}} \cap \Omega_{\mathtt{pml}}$ is assumed to be placed at coordinates x_0 and y_0, see Figure 1. Note from this figure that the function σ_x is computed with $x_0 = x_0^{\mathtt{L}}$ for $\Omega^{\mathtt{L}x}_{\mathtt{pml}}$, and with $x_0 = x_0^{\mathtt{R}}$ for $\Omega^{\mathtt{R}x}_{\mathtt{pml}}$. Note that in the interior domain the PML model does not change the original Mild-Slope Equations (MSE), recall Eq. (1), since $\sigma_x = \sigma_y = 0$ at any point $(x, y) \in \Omega_{\mathtt{int}}$.

Eq. (6c) is a first-order *non-reflecting boundary condition* (Givoli 1992) on the PML outer boundary, and it is used to minimize spurious reflections. Other artificial conditions can be also used but, in practice, a proper choice of the absorbing parameters usually makes the solution not sensitive to the type of artificial boundary condition used on $\Gamma_{\mathtt{pml}}$.

Finally, it is important to note that the PML model (6) behaves as a perfectly absorbing layer (i.e. it reproduces the original semi-infinite solution of Eq. (1)) only if the following

condition is satisfied: for any point in the PML region $\Omega_{\texttt{pml}}$, the MSE (1) formulated in terms of the scattered wave must be homogeneous along the absorbing directions (x and y). That is, the scattered wave formulation particularized at the PML must have: (i) null source term, (ii) constant coefficients along the x direction in $\Omega^{\texttt{L}x}_{\texttt{pml}} \cup \Omega^{\texttt{R}x}_{\texttt{pml}} \cup \Omega^{x,y}_{\texttt{pml}}$, and (iii) constant coefficients along the y direction in $\Omega^{y}_{\texttt{pml}} \cup \Omega^{x,y}_{\texttt{pml}}$. Otherwise, the absorption properties of the artificial layer are not guaranteed, see Oskooi et al. (2008) and Oskooi and Johnson (2011) for details. It is straightforward to verify that these conditions are attained if:

(i) The incident wave ϕ_0 verifies the MSE (1) in the absorbing layer, that is

$$\boldsymbol{\nabla} \cdot (c\, c_g \boldsymbol{\nabla} \phi_0) + k^2 c\, c_g \phi_0 = 0 \quad \text{in } \Omega_{\texttt{pml}}. \tag{9}$$

(ii) The exterior bathymetry satisfies Eq. (5).

Details on the PML derivation are shown in the Appendix. Next Section shows how the incident wave can be rapidly determined at any point $(x, y) \in \Omega_{\texttt{pml}}$ accordingly to Eq. (9). This follows the rationale proposed by Panchang et al. (2000).

Computation of the incident wave field

Note that Eq. (6) requires the expression of the incident wave only in the PML. In the far-field bathymetry region, the incident wave is defined as a monochromatic wave with an incoming angle $\theta \in \mathbb{R}$ and amplitude A_0, namely

$$\phi_0(x, y) = A_0 \exp(ik_0 x \cos\theta) \exp(ik_0 y \sin\theta) \quad \text{if } (x, y) \in \Omega^{y}_{\texttt{pml}} \cup \Omega^{x,y}_{\texttt{pml}}, \tag{10}$$

where k_0 is the wavenumber from (2) with $h = h_0$. Note that ϕ_0, as defined by (10), verifies Eq. (9) with constant coefficients (i.e. the Helmholtz equation) in $\Omega^{y}_{\texttt{pml}} \cup \Omega^{x,y}_{\texttt{pml}}$. In the rest of the PML region the bathymetry depends only on coordinate y and is constant in the x (alongshore) direction. The procedure to compute ϕ_0 in this case consists in looking for an

incident wave with the same factorized structure as Eq. (10), that is

$$\phi_0(x,y) = \exp(ik_0 x\cos\theta)\tilde{\phi}_0(y), \tag{11}$$

where $\tilde{\phi}_0$ is the cross-shore part of ϕ_0. Substituting Eq. (11) in (9), and using proper boundary conditions, the function $\tilde{\phi}_0$ can be found as the solution of the second-order ordinary differential equation

$$\frac{\partial}{\partial y}\left(c\,c_g\frac{\partial\tilde{\phi}_0}{\partial y}\right) + \tilde{k}^2\,c\,c_g\tilde{\phi}_0 = 0 \quad \text{in } y\in]y_c, y_0[, \tag{12a}$$

$$\tilde{\phi}_0(y_0) = A_0\exp(ik_0 y_0\sin\theta), \tag{12b}$$

$$\frac{\partial\tilde{\phi}_0}{\partial y}(y_c) + ik\,\tilde{\phi}_0(y_c) = 0, \tag{12c}$$

where $\tilde{k} = \sqrt{k^2 - k_0^2\cos^2\theta}$ is the associated wavenumber. Recall that parameters c, c_g and k depend only on coordinate y. The limits for the range of y, y_0 and y_c, correspond to the position of the far-field region and the coastline, respectively, see Figure 1. Note that boundary condition (12b) imposes continuity at the far-field region. On the other hand, Eq. (12c) corresponds to the one-dimensional version of the first-order artificial condition used in Eq. (6c). It imposes that the incident wave is not influenced by the harbor. No spurious reflections of $\tilde{\phi}_0$ are produced because the direction of incidence is obviously normal, and the first-order condition becomes in this case exact.

It is important to note that a distinguishing aspect of the proposed model is the possibility of using two different bathymetries in the regions $\Omega^{\mathtt{L}x}_{\mathtt{pml}}$ and $\Omega^{\mathtt{R}x}_{\mathtt{pml}}$, which can have also two different coastline positions, see Figure 1. This requires solving two times the ordinary differential equation (12): one using $y_c = y_c^{\mathtt{L}}$ and the coefficients induced by the bathymetry $h^{\mathtt{L}}(y)$, and another using $y_c = y_c^{\mathtt{R}}$ and coefficients corresponding to $h^{\mathtt{R}}(y)$. Note that a large distance between the two PML regions $\Omega^{\mathtt{L}x}_{\mathtt{pml}}$ and $\Omega^{\mathtt{R}x}_{\mathtt{pml}}$ reduces the impact of the idealization of the bathymetry, allowing better representations of the real semi-infinite domain. This

is a more realistic approximation than the standard used in elliptic harbors models, in which either a unique cross-shore variation represents the whole exterior bathymetry, or interpolation is required at the open boundary, see for instance Zhao et al. (2001) and Chen et al. (2005).

VALIDATION OF THE PML MODEL

Three academic tests and one realistic example are considered next. The quantity of interest used in all the examples is the amplification factor (i.e. normalized wave height), namely

$$H(x, y) = |\phi|/A_0. \tag{13}$$

The parameters of the PML have to be specified first. Recall that these parameters are required for the definition of the absorbing functions in Eq. (8). Here, absorption degree $n = 2$ is always used and the PML thickness $L_{\texttt{pml}}$ is selected as 1.5 times the maximum wave length induced by the lower frequency in each example, see Michler et al. (2007). The last PML parameter, σ_0, is set to $\sigma_0 = 60$ following the values proposed by Collino and Monk (1998) that maximize the damping in the absorbing medium.

In general, the following examples use fourth-order triangular finite element meshes adapted to the bathymetry, in order to achieve 8 nodes per wavelength over all the computational domain. Fourth-order elements are employed because of their numerical performance, as demonstrated in the comparison study by Giorgiani et al. (2013). The complex linear system resulted from this discretization is solved by means of direct methods.

Circular scattering with constant bathymetry

A standard test for open boundaries is first studied. The geometry is a reflecting circular obstacle of radius R_c located with a distance R_d from the upper PML domain, as shown in the left panel of Figure 2. These tests are standard to study the accuracy of the artificial layers. The example consists in the scattering of an incident wave of period $T = 2\pi/\omega = 10$ s that propagates with an incoming angle $\theta = 0$. In this example the bathymetry is constant

in all the computational domain with value $h = 15.0119$ m from Panchang et al. 2000. The analytical solution for this problem is available in Mei (1983).

The computed amplification factor is depicted in Figure 2. Particularly, the left panel shows the case $R_d/R_c = 10$ and the right panel considers $R_d/R_c = 2$ with a not centered circle very close to the absorbing region. Note that the proximity of the PML does not perturb the symmetry of the solution. The relative error map between numerical and exact amplification factors (i.e. H and $H^{\texttt{exact}}$ resp.) is depicted in Figure 3 for both cases, that is $|H - H^{\texttt{exact}}|/H^{\texttt{exact}}$, see Eq. (13). The maximum errors are on the order of 10^{-4}, that indicates an excellent agreement with the analytical solution even with a very close PML region.

This result outperforms previous harbor models based on the exterior description of the scattered wave, see for instance Panchang et al. (2000). Moreover, in order to be more confident about the reliability of the model, the convergence of the solution along the circle boundary ($\Gamma_{\texttt{R}}$) is shown in Figure 4. It is constructed by measuring the $\mathcal{L}^2$ norm of the relative error between approximation (ϕ) and exact solution ($\phi^{\texttt{exact}}$) for different mesh sizes, namely

$$E^2 = \frac{\int_{\Gamma_{\texttt{R}}} (\phi - \phi^{\texttt{exact}})(\overline{\phi - \phi^{\texttt{exact}}})\, d\Gamma}{\int_{\Gamma_{\texttt{R}}} \phi^{\texttt{exact}} \overline{\phi^{\texttt{exact}}}\, d\Gamma}, \tag{14}$$

where the overline denotes the complex conjugate. High fidelity predictions (error level around 10^{-6}) are achieved, and the convergence rate for fourth-order finite elements is well reproduced in both tests (Babuška and Suri 1987). This corroborates the excellent behavior of the PML open boundary for constant bathymetry, even when it is placed in the vicinity of the obstacle.

Semicircular scattering with variable bathymetry

A scattering problem in a semi-infinite domain with variable bathymetry is explored next. The objective of this test is to show the ability of the proposed formulation to cope with two different bathymetries at the left and right boundaries. Furthermore, it is used to analyze

how the distance to the artificial boundary influences the results in an area of interest.

The geometry consists in a totally reflective boundary (i.e. $\alpha = 0$), including a semicircle of radius R_c, which is adjacent to an absorbing boundary of length D_1. The interior domain is then limited by the vertical distance D_2. Note from Figure 5 that distances D_1 and D_2 define the position of the PML in the geometry. The dimensionless variables $x' = x/R_c$, $y' = y/R_c$, $D_1' = D_1/R_c$ and $D_2' = D_2/R_c$ are henceforth used. The bathymetry ranges as $0.01 \leq h(x', y') \leq 0.3$ with $h(x', y') = 0.145y' + 0.053x' + 0.115$ in the region $-2 \leq x' \leq 2$, and it becomes constant in the x' direction otherwise. This leads to two different cross-shore bathymetries in the left and right regions, $x' < -2$ and $x' > 2$, respectively. Two oblique incoming angles $\theta = \{220°, 310°\}$ and period $T = 0.6$ s are considered for testing the open boundary.

The incident wave field is computed in the PML accordingly to Eq. (12) for each cross-shore bathymetry. Exterior bathymetry effects are observed in the left region (see Figure 5), whereas the right cross-shore bathymetry does not induce noticeable refractions on the far-field incident wave. Moreover, note from Figure 5 that this example induces strong reflections in the distribution of the amplification factor. Obviously, these large values of the wave amplification are inherent of this geometry (it presents a corner between two totally reflective boundaries) and incoming wave direction. However, this does not influence the purpose of this study because the unphysical amplification factors (i.e. larger than 3) are independent of the PML application. In fact, this problem highlights the applicability and excellent performance of the proposed PML method for problems with two different exterior bathymetries.

In order to evaluate the influence of the PML in the solution of the problem, a set of computations with the same mesh size but different combinations of D_1' and D_2' are performed. Specifically, fourth order uniform meshes with a minimum resolution of 16 nodes per wavelength are employed. Since there is no analytical solution for this problem, a reference computation with $D_1' = D_2' = 4$ and half of the element size is used to evaluate

the error. On the semicircle boundary, named as Γ, the following errors in the amplification factor are defined: the mean error

$$E_1^2 = \frac{1}{\text{meas}(\Gamma)} \int_\Gamma (H^* - H)^2 \, d\Gamma, \tag{15}$$

and the maximum elemental error, namely

$$E_2^2 = \max_{\forall \Gamma_i \subset \Gamma} \frac{1}{\text{meas}(\Gamma_i)} \int_{\Gamma_i} (H^* - H)^2 \, d\Gamma, \tag{16}$$

where H is the computed (approximated) amplification factor, as defined in Eq. (13), and H^* is the reference solution. Each Γ_i is the side of a finite element along Γ.

These errors are depicted in Figure 6 for a variety of values of D_1' and D_2'. For both mean and maximum errors, the parameter D_2' that stands for the PML position in the far-field (constant) bathymetry region has no influence on the solution along the semicircle boundary. The errors are measured on the semicircular scatterer, if the incoming wave angle is $\theta = 220°$ waves are only slightly refracted and D_2' may seem not very influential. Thus, an incoming wave angle $\theta = 310°$ is also tested and the errors plotted, see Figure 6 (right).

The results produced by the parameter D_2' are in agreement to the conclusions of the previous example in which the bathymetry was also constant. In fact, the far-field PML region can be placed at a minimum (optimal) distance of $D_2' = 0$. As expected, this behavior is not reproduced for the parameter D_1' defining the PML position in the variable bathymetry regions. Nevertheless, it is observed that using only $D_1' = 1$, and hence with the PML very close to the obstacle, is sufficient to ensure that even the maximum elemental error is no longer (significantly) perturbed. As seen in Figure 6, for $D_1' > 1$ the error is almost constant and only due to the finite element discretization. It is important to remark that each dot in Figure 6 represents a finite element computation for a given value of D_1' and D_2'. These computation are done with finite element meshes with the same characteristic element size (same error bound) but not with identical meshes around the semi-circular

scatterer (the nodes are not exactly in the same position in the smaller interior domain defined by $D'_1 = D'_2 = 0$). This induces negligible differences that are more evident when the curve flattens, that is, when the PML error is negligible compared with the finite element one (the discretization error).

In order to obtain more information on the PML influence, Figure 7 depicts the accuracy of the computed amplification factor in the smaller interior domain (defined by $D'_1 = D'_2 = 0$). Accuracy is shown by the number of correct significant digits of the solution (see Remark 1). The isolines of amplification factor equal to one ($H = 1$) for both the computed and reference solutions are also shown. In the three depicted computations, $D'_2 = 0$ is selected since this parameter has not significant influence on the results. Convergence to the reference solution when increasing the value of D'_1 is observed. Note that the area within the isoline of one correct digit of accuracy decreases as D'_1 increases. The case $D'_1 = 1$, that provides the optimal PML position when measuring the global error on the circle, produces an accuracy of one correct significant digit in almost all the area of interest. The regions with no accuracy are negligible and almost disappear as D'_1 increases. Consequently, in this synthetic problem with non-constant exterior (idealized) bathymetry, the PML is also able to reproduce the semi-infinite solution using a small computational domain.

Remark 1 (Correct significant digits of the solution)**.** Numerical accuracy can be evaluated by estimating the number of correct significant digits (or correct significant figures) between approximation (ϕ) and reference solution ($\phi^{\mathtt{ref}}$). An approximation has q significants digits if the relative error, namely $e = (\phi - \phi^{\mathtt{ref}})/\phi^{\mathtt{ref}}$, verifies $|e| < 0.5 \times 10^{-q}$, or alternatively, $q = -\log_{10}|e|$, see Higham (2002). That is, the first nonzero digit of the approximation and up to q succeeding digits can be "trusted". From Higham (2002): "an approximation ϕ to $\phi^{\mathtt{ref}}$ has q correct significant digits if ϕ and $\phi^{\mathtt{ref}}$ round to the same number to q significant digits". Note that applications for harbor agitation usually do not demand more than $q = 2$.

Elliptic shoal

The elliptic shoal is a well-known test case largely used to validate models in coastal regions. It consists in testing the refraction effects produced by a shoal located into a mild-sloped bathymetry plane. Although this example does not present large wave reflections, it has been used here to validate the proposed methodology with reference experimental and numerical results. The definition of the bathymetry and shoal limits can be found, for instance, in Belibassakis et al. (2001).

The results of this test (not shown) were nearly identical to those in Oliveira and Anastasiou (1998) and Panchang et al. (1991). That is, it performs fairly well within the limitations of the linear wave theory, that usually over-predicts the energy concentration associated to the shoal refraction. Nonlinear wave models, see for instance Woo and Liu (2004), can be used to drastically improve the wave description in this particular test.

Mataró Harbor

This example is presented to show the applicability and reliability of the proposed model for more complex problems. The real geometry and bathymetry of the Mataró harbor, located in the Northeast of Spain, are considered. Figure 8 shows three computational domains used for comparison purposes. The small domain hardly includes the exterior part of the harbor and it produces a 80% of reduction in degrees of freedom (DOF) with respect to the largest domain, and 40% with respect to the medium domain. The medium computational domain (60 000 DOF) has a 70% of reduction with respect to the largest domain and is probably a reasonable engineering option. Note that the largest domain is used to obtain a reference solution for this problem, and it incorporates the real bathymetry and coastlines. Nevertheless, both small and medium domains are drastically smaller than the reference one and they include two different exterior bathymetries with completely non-collinear coastlines. Note also from Figure 8 that models requiring collinear coastlines cannot reproduce the real geometry using small domains. In terms of the computational time required to solve this problem (assembling of matrices and solution of linear systems), the

medium and small domains, respectively, use the 29% and 17% of the CPU time demanded by the largest domain.

The absorbing coefficient α in Eq. (3) is specified in Figure 8 for all the boundaries of the medium computational domain. The rest of boundaries correspond to the case $\alpha = 0.7$. For each domain, both short (6 s) and longer (16 s) incident waves are used in the computations accordingly to those limit values observed offshore in the region. Two different incoming directions, $\theta = 270^\circ$ and $\theta = 225^\circ$, are also considered to cover normal and oblique incident waves. A particular solution of the amplification factor for the shorter and oblique incident waves is depicted in Figure 8.

In order to test the model performance, three different sections of interest are defined in the harbor (see the medium computational domain in Figure 8). Results of the amplification factor on these sections, for shorter and longer waves, are depicted in Figures 9 and 10, respectively. In each figure, the top row depicts the comparison between different domains for the normal incoming wave direction, whereas the bottom row shows the oblique case.

In general, the small domain produces reasonably good results, under engineering tolerance, following the trend of the reference solution specially for the wave phase. This indicates that PML is able to reproduce the exterior effects, even though it only uses a very small region of the exterior part of the harbor. It is also observed that the medium domain reduces the error in almost all the cases. The minor differences are observed for the shorter and normal incident waves (top row in Figure 9), because under these circumstances the influence of the exterior part of the harbor decreases considerably on the sections of interest. As expected, the oblique incoming direction induces larger errors (bottom row in Figure 9). In general, the smaller domain slightly underestimates the wave amplification. Note that the medium domain produces very satisfactory results even for the oblique case.

The longer waves case is specially interesting because the exterior bathymetry produces more refractions than for short waves. A comparison is depicted in Figure 11 for the computed incident wave. In previous models based on the exterior description of the scattered

wave, these refractions induce higher errors in the computations associated to large wave periods, see Panchang et al. (2000). Here, the results from Figure 10 show that the differences with respect to the reference solution are similar to the short waves case. This indicates less sensitivity of the PML model to variations on the wave period.

CONCLUDING REMARKS

The Perfectly Matched Layer method is proposed to model an artificial non-reflecting boundary for elliptic harbor models. A rectangular shaped absorbing layer is introduced, and the linear Mild-Slope equation is used to describe the wave physics in the harbor. Exterior refractions are incorporated into the model by using a natural simplification of the exterior domain, geometry and bathymetry. Particularly, the exterior bathymetry is considered constant only in the alongshore direction. As a result of this not very restrictive assumption, the incident wave is efficiently computed in the absorbing region as the solution of a one-dimensional problem. Moreover, and in opposite to standard strategies, two exterior bathymetries are used with two non-collinear coastlines, in order to more accurately approximate the real unbounded domain.

Results show that solutions are not significantly perturbed even with close placed artificial boundaries. This is specially evident in the far-field constant bathymetry area of the model. In this case, the top part of the PML is placed practically on the limit of constant bathymetry.

The proposed model is promising also for more complex problems. For a real case, the model produces good results with a computational domain that hardly involves the exterior part of the harbor. This is observed even with an oblique incoming wave direction and a large period. Reliable solutions of the harbor agitation are therefore obtained at a reduced computational cost. Future advancements include the use of the PML in more sophisticated propagation models for harbor agitation, including non-linear wave interactions.

APPENDIX I. DERIVATION OF THE PML

This appendix describes the derivation of Eq. (6a) in the PML. The original rationale from Berenger (1994) imposes the absorption of the scattered wave through the transient

wave propagation solution, although other methods can be used to obtain the same equation, see Chew et al. (1997). The original rationale is followed here.

In the PML, the transient Mild-Slope equation, where $\tilde{\phi}_s(x,y,t) = \phi_s(x,y)e^{-i\omega t}$ is the monochromatic scattered wave and $\phi_s = \phi - \phi_0$, can be written as

$$\frac{\partial^2 \tilde{\phi}_s}{\partial t^2} - \frac{c}{c_g}\boldsymbol{\nabla}\cdot(cc_g\boldsymbol{\nabla}\tilde{\phi}_s) = 0 \quad \text{in } \Omega_{\texttt{pml}}. \tag{17}$$

Note that null RHS is imposed because the incident wave fulfills the equation in the PML, recall Eq. (9). The change of variables

$$\tilde{v} = \frac{\partial \tilde{\phi}_s}{\partial t}, \quad \tilde{q}_x = \frac{\partial \tilde{\phi}_s}{\partial x}, \quad \tilde{q}_y = \frac{\partial \tilde{\phi}_s}{\partial y}, \tag{18}$$

and the decomposition $\tilde{v} = \tilde{v}_x + \tilde{v}_y$ lead to the first order system

$$\frac{\partial \tilde{v}_x}{\partial t} = \frac{c}{c_g}\frac{\partial}{\partial x}(cc_g\tilde{q}_x), \tag{19a}$$

$$\frac{\partial \tilde{q}_x}{\partial t} = \frac{\partial \tilde{v}_x}{\partial x} + \frac{\partial \tilde{v}_y}{\partial x}, \tag{19b}$$

$$\frac{\partial \tilde{v}_y}{\partial t} = \frac{c}{c_g}\frac{\partial}{\partial y}(cc_g\tilde{q}_y), \tag{19c}$$

$$\frac{\partial \tilde{q}_y}{\partial t} = \frac{\partial \tilde{v}_x}{\partial y} + \frac{\partial \tilde{v}_y}{\partial y}. \tag{19d}$$

This system provides a solution for Eq. (17). Note that Eqs. (19a) and (19b) describe the propagation of $\tilde{v}_x$ and $\tilde{q}_x$, respectively, along the x direction. Analogously, Eqs. (19c) and (19d) describe the propagation of $\tilde{v}_y$ and $\tilde{q}_y$ along the y direction. Note, moreover, that Eqs. (19a) and (19c) are fully homogeneous (constant cc_g) in the PML along their directions because of the bathymetry restriction (5). The main point of the PML resides in modifying the original system (19) with a damping term in each direction that vanishes outside the

PML, that is

$$\frac{\partial \tilde{v}_x}{\partial t} + \sigma_x \tilde{v}_x = \frac{c}{c_g}\frac{\partial}{\partial x}(cc_g\tilde{q}_x), \tag{20a}$$

$$\frac{\partial \tilde{q}_x}{\partial t} + \sigma_x \tilde{q}_x = \frac{\partial \tilde{v}_x}{\partial x} + \frac{\partial \tilde{v}_y}{\partial x}, \tag{20b}$$

$$\frac{\partial \tilde{v}_y}{\partial t} + \sigma_y \tilde{v}_y = \frac{c}{c_g}\frac{\partial}{\partial y}(cc_g\tilde{q}_y), \tag{20c}$$

$$\frac{\partial \tilde{q}_y}{\partial t} + \sigma_y \tilde{q}_y = \frac{\partial \tilde{v}_x}{\partial y} + \frac{\partial \tilde{v}_y}{\partial y}, \tag{20d}$$

where $\sigma_x(x)$ and $\sigma_y(y)$ are defined in Eq. (8). The frequency domain version of this system considers a monochromatic definition of the unknowns, namely $\tilde{v}(x,y,t) = v(x,y)e^{-i\omega t}$, $\tilde{q}_x(x,y,t) = q_x(x,y)e^{-i\omega t}$ and $\tilde{q}_y(x,y,t) = q_y(x,y)e^{-i\omega t}$. System (20) is then rewritten as

$$\begin{aligned}
(-i\omega + \sigma_x)v_x &= \frac{c}{c_g}\frac{\partial}{\partial x}(cc_g q_x),\\
-i\omega q_x &= \frac{1}{s_x}\left(\frac{\partial v_x}{\partial x} + \frac{\partial v_y}{\partial x}\right),\\
(-i\omega + \sigma_y)v_y &= \frac{c}{c_g}\frac{\partial}{\partial y}(cc_g q_y),\\
-i\omega q_y &= \frac{1}{s_y}\left(\frac{\partial v_x}{\partial y} + \frac{\partial v_y}{\partial y}\right),
\end{aligned}$$

where $s_x = 1 + i\sigma_x/\omega$ and $s_y = 1 + i\sigma_y/\omega$. After rearranging all these equations and using the decomposition $v = v_x + v_y$ and the change of variables (18), the following equation for the scattered wave $\phi_s(x,y)$ arises

$$-\frac{c_g}{c}\omega^2\phi_s = \frac{1}{s_x}\left(\frac{cc_g}{s_x}\frac{\partial \phi_s}{\partial x}\right) + \frac{1}{s_y}\left(\frac{cc_g}{s_y}\frac{\partial \phi_s}{\partial y}\right) \quad \text{in } \Omega_{\texttt{pml}}. \tag{22}$$

Taking into account that $k = \omega/c$ and $\phi = \phi_s + \phi_0$, the Mild-Slope equation (6a) is obtained.

ACKNOWLEDGMENTS

This work has been partially supported by the Spanish Ministry of Science and Competitiveness, grants number: DPI2011-27778-C02-02 and DPI2014-51844-C2-02, and the Catalan

Government, grant number: 2009SGR875.

REFERENCES

Babuška, I. and Suri, M. (1987). "The optimal convergence rate of the p-version of the finite element method." *SIAM J. Numer. Anal.*, 24(4), 750–776.

Basu, U. and Chopra, A. K. (2003). "Perfectly matched layers for time-harmonic elastodynamics of unbounded domains: Theory and finite-element implementation." *Comput. Methods Appl. Mech. Eng.*, 192(11-12), 1337–1375.

Belibassakis, K. A., Athanassoulis, G. A., and Gerostathis, T. P. (2001). "A coupled-mode model for the refraction-diffraction of linear waves over steep three-dimensional bathymetry." *Appl. Ocean Res.*, 23(6), 319–336.

Berenger, J.-P. (1994). "A perfectly matched layer for the absorption of electromagnetic waves." *J. Comput. Phys.*, 114(2), 185–200.

Berkhoff, J. C. W. (1972). "Computation of combined refraction-diffraction." *Proc. 13th Coastal Engineering Conference*, Vol. 1, Vancouver, Canada. 471–490.

Booij, N. (1981). "Gravity waves on water with non-uniform depth and current." *Report No. 81-1*, Department of Civil Engineering, Delft University of Technology, The Netherlands.

Chen, W., Panchang, V., and Demirbilek, Z. (2005). "On the modeling of wave-current interaction using the elliptic mild-slope wave equation." *Ocean Eng.*, 32(17-18), 2135–2164.

Chew, W. C., Jin, J. M., and Michielssen, E. (1997). "Complex coordinate stretching as a generalized absorbing boundary condition." *Microw. Opt. Technol. Lett.*, 15(6), 363–369.

Collino, F. and Monk, P. (1998). "Optimizing the perfectly matched layer." *Comput. Methods Appl. Mech. Eng.*, 164(1–2), 157–171.

Demaldent, E. and Imperiale, S. (2013). "Perfectly matched transmission problem with absorbing layers: Application to anisotropic acoustics in convex polygonal domains." *Int. J. Numer. Methods Eng.*, 96(11), 689–711.

Giorgiani, G., Modesto, D., Fernández-Méndez, S., and Huerta, A. (2013). "High-order con-

tinuous and discontinuous Galerkin methods for wave problems." *Int. J. Numer. Methods Fluids*, 73(10), 883–903.

Givoli, D. (1992). *Numerical methods for problems in infinite domains*, Vol. 33 of *Studies in Applied Mechanics*. Elsevier Scientific Publishing Co., Amsterdam.

Higham, N. J. (2002). *Accuracy and Stability of Numerical Algorithms*. Society for Industrial and Applied Mathematics, Philadelphia, PA, USA.

Kirby, J. T. (1984). "Note on linear surface wave-current interaction over slowly varying topography." *J. Geophys. Res.*, 89(NC1), 745–747.

Larsen, J. and Dancy, H. (1983). "Open boundaries in short wave simulations - A new approach." *Coast. Eng.*, 7(3), 285–297.

Lee, C. and Yoon, S. B. (2004). "Effect of higher-order bottom variation terms on the refraction of water waves in the extended mild-slope equations." *Ocean Eng.*, 31(7), 865–882.

Li, D., Panchang, V., Tang, Z., Demirbilek, Z., and Ramsden, J. (2005). "Evaluation of an approximate method for incorporating floating docks in harbor wave prediction models." *Can. J. Civ. Eng.*, 32(6), 1082–1092.

Massel, S. R. (1993). "Extended refraction-diffraction equation for surface waves." *Coast. Eng.*, 19(1-2), 97–126.

Mei, C. C. (1983). *The applied dynamics of ocean surface waves*. Wiley, New York.

Michler, C., Demkowicz, L., Kurtz, J., and Pardo, D. (2007). "Improving the performance of perfectly matched layers by means of hp-adaptivity." *Numer. Meth. Part. Differ. Equ.*, 23(4), 832–858.

Modesto, D., Zlotnik, S., and Huerta, A. (2015). "Proper generalized decomposition for parameterized Helmholtz problems in heterogeneous and unbounded domains: Application to harbor agitation." *Comput. Methods Appl. Mech. Eng.*, 295, 127–149.

Navon, I. M., Neta, B., and Hussaini, M. Y. (2004). "A perfectly matched layer approach to the linearized shallow water equations models." *Mon. Wea. Rev.*, 132(6), 1369–1378.

Oliveira, F. S. B. F. and Anastasiou, K. (1998). "An efficient computational model for water wave propagation in coastal regions." *Appl. Ocean Res.*, 20(5), 263–271.

Oskooi, A. and Johnson, S. G. (2011). "Distinguishing correct from incorrect PML proposals and a corrected unsplit PML for anisotropic, dispersive media." *J. Comput. Phys.*, 230(7), 2369–2377.

Oskooi, A. F., Zhang, L., Avniel, Y., and Johnson, S. G. (2008). "The failure of perfectly matched layers, and towards their redemption by adiabatic absorbers." *Opt. Exp.*, 16(15), 11376–11392.

Panchang, V., Chen, W., Xu, B., Schlenker, K., Demirbilek, Z., and Okihiro, M. (2000). "Exterior bathymetric effects in elliptic harbor wave models." *J. Waterw. Port Coast. Ocean Eng.*, 126(2), 71–78.

Panchang, V., Pearce, B., Wei, G., and Cushman-Roisin, B. (1991). "Solution of the mild-slope wave problem by iteration." *Appl. Ocean Res.*, 13(4), 187–199.

Panchang, V., Zhang, J., and Demirbilek, Z. (2008). "Incorporating rubble mound jetties in elliptic harbor wave models." *J. Waterw. Port Coast. Ocean Eng.*, 134(1), 40–52.

Sharma, A., Panchang, V., and Kaihatu, J. (2014). "Modeling nonlinear wavewave interactions with the elliptic mild slope equation." *Appl. Ocean Res.*, 48, 114–125.

Singer, I. and Turkel, E. (2004). "A perfectly matched layer for the Helmholtz equation in a semi-infinite strip." *J. Comput. Phys.*, 201(2), 439–465.

Teixeira, F. L. and Chew, W. C. (2000). "Complex space approach to perfectly matched layers: a review and some new developments." *Int. J. Numer. Model. Electron. Networks*, 13(5), 441–455.

Tsay, T.-K. and Liu, P. L.-F. (1983). "A finite element model for wave refraction and diffraction." *Appl. Ocean Res.*, 5(1), 30–37.

Wei, G. and Kirby, J. T. (1995). "Time-dependent numerical code for extended Boussinesq equations." *J. Waterw. Port Coast. Ocean Eng.*, 121(5), 251–261.

Woo, S.-B. and Liu, P. L.-F. (2004). "Finite-element model for modified Boussinesq equa-

525 tions. I: Model development." *J. Waterw. Port Coast. Ocean Eng.*, 130(1), 1–16.
526 Xu, B. and Panchang, V. (1993). "Outgoing Boundary Conditions for Finite-Difference El-
527 liptic Water-Wave Models." *Proc. R. Soc. London Ser. A*, 441(1913), 575–588.
528 Xu, B., Panchang, V., and Demirbilek, Z. (1996). "Exterior reflections in elliptic harbor
529 wave models." *J. Waterw. Port Coast. Ocean Eng.*, 122(3), 118–126.
530 Zhao, L., Panchang, V., Chen, W., Demirbilek, Z., and Chhabbra, N. (2001). "Simulation of
531 wave breaking effects in two-dimensional elliptic harbor wave models." *Coast. Eng.*, 42(4),
532 359–373.
533 Zubier, K., Panchang, V., and Demirbilek, Z. (2003). "Simulation of waves at duck (North
534 Carolina) using two numerical models." *Coast. Eng. J.*, 45(3), 439–469.

List of Figures

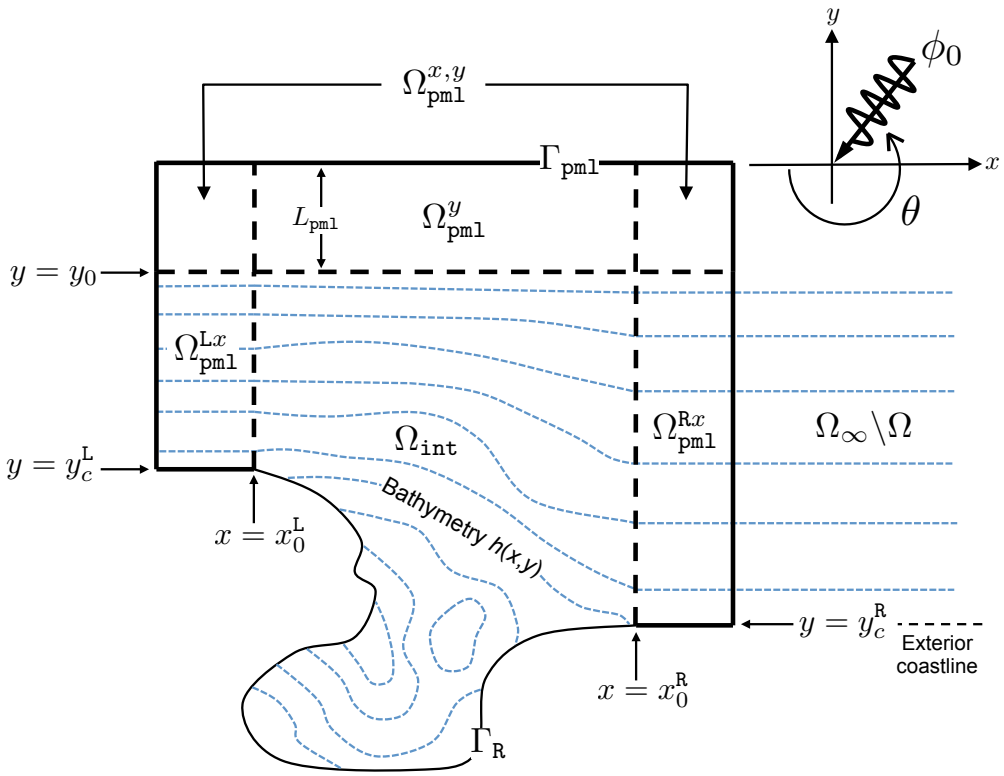

FIG. 1. Sketch of the harbor model: computational domain with PML and idealization of the exterior bathymetry.

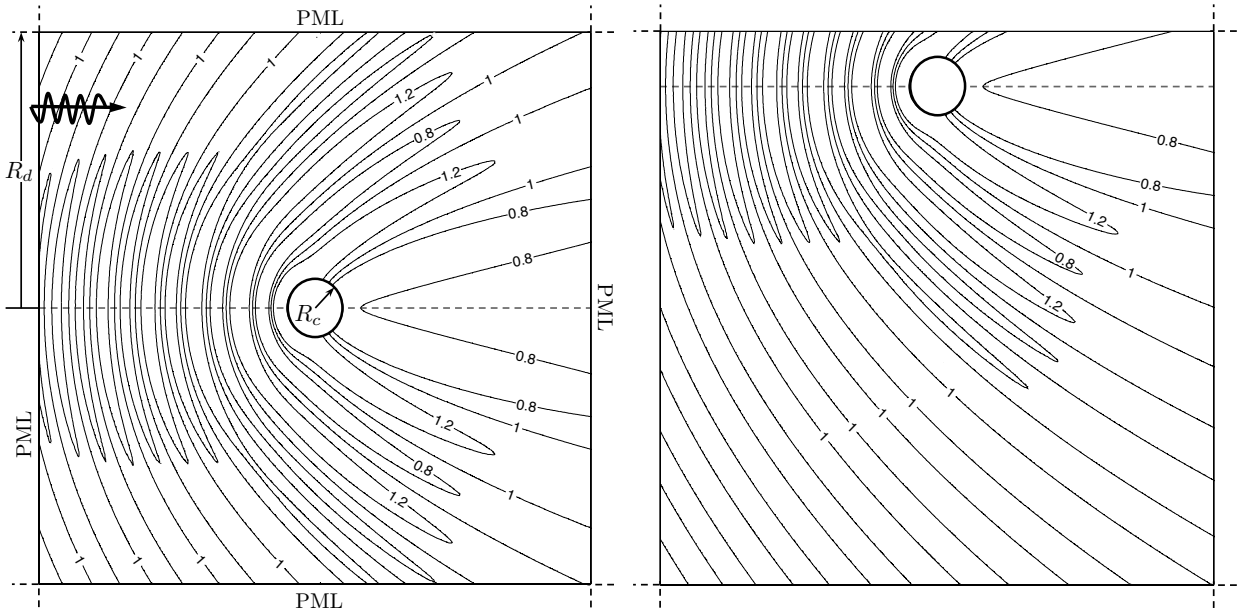

FIG. 2. Circular scattering with constant bathymetry: isolines of the amplification factor of the numerical solution for a centered circled obstacle (left) and for a not centered one (right). The dashed line indicates the position of the symmetry axis.

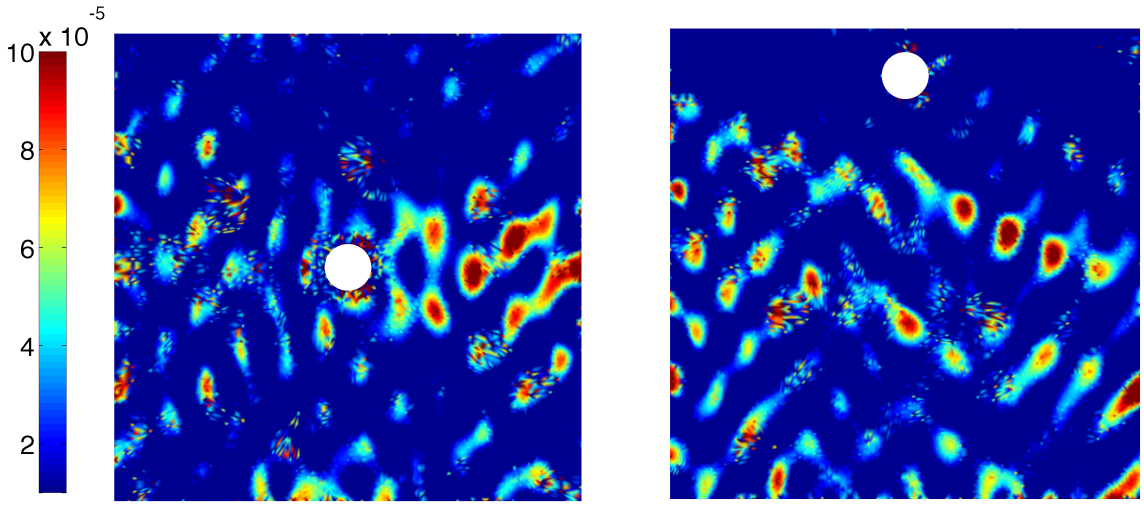

FIG. 3. Circular scattering with constant bathymetry: relative error of the amplification factor ($|H - H^{\texttt{exact}}|/H^{\texttt{exact}}$) for a centered circled obstacle (left) and for a not centered one (right).

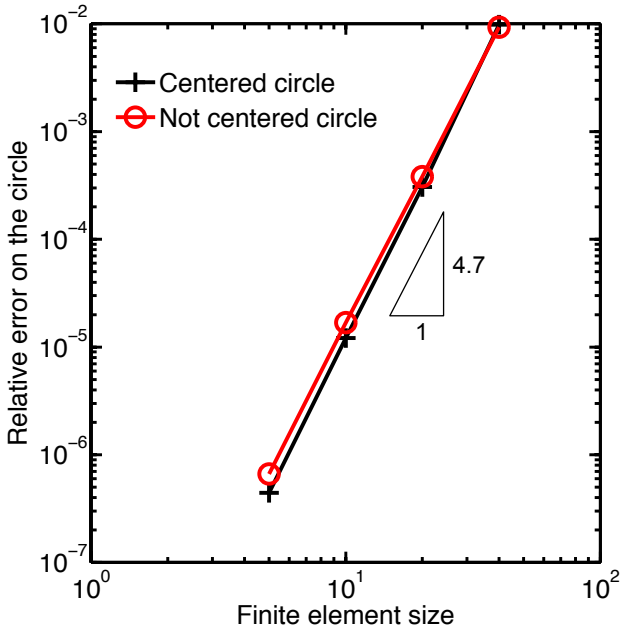

FIG. 4. Circular scattering with constant bathymetry: convergence of the $\mathcal{L}^2$ norm of the error, see Eq. (14), along the circle boundary. Four-order finite elements are used and mean convergence rate is reported.

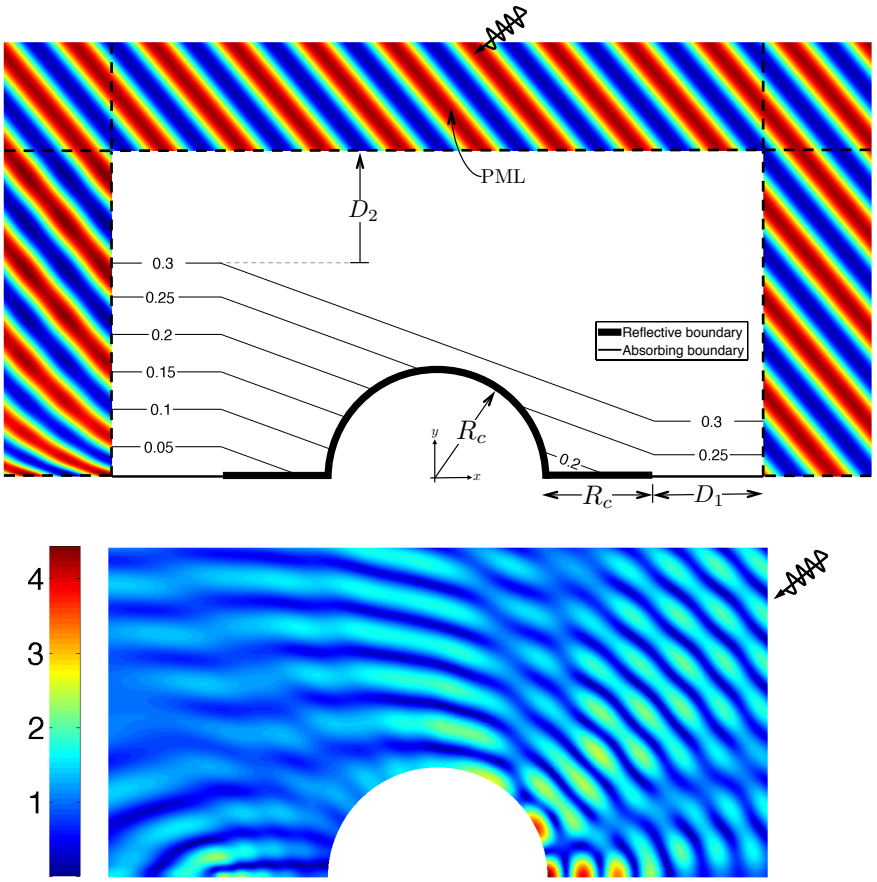

FIG. 5. Semicircular scattering with variable bathymetry: problem statement (top) and distribution of the amplification factor with an incoming wave angle $\theta = 220°$ (bottom). The incident wave field (0.6 s of period) is also depicted (top) in the PML artificial layer accordingly to each of the two cross-shore bathymetries.

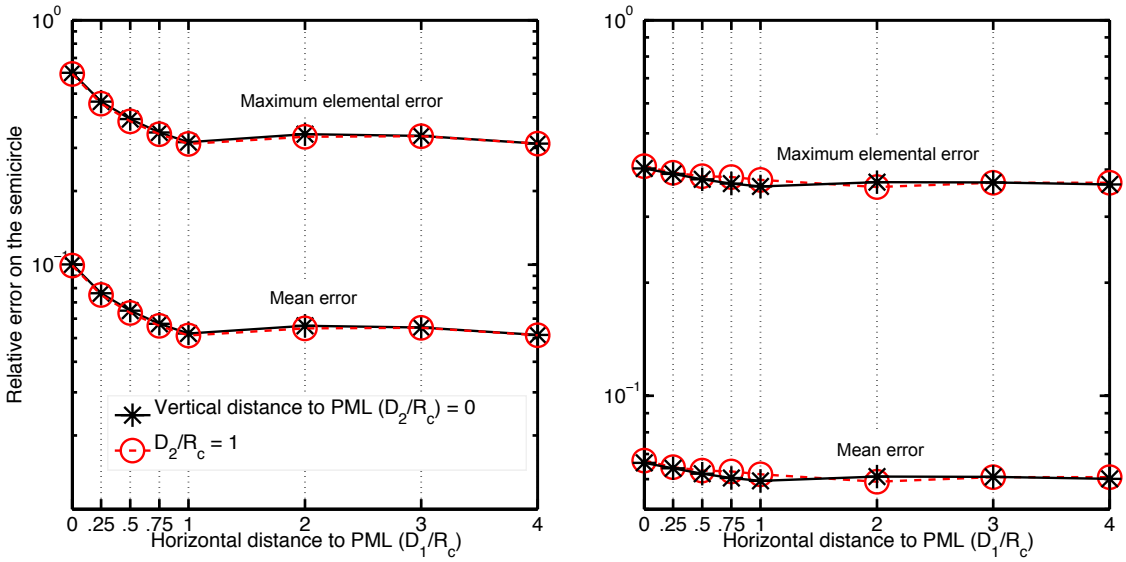

FIG. 6. Semicircular scattering with variable bathymetry: PML influence on the amplification factor along the semicircle obstacle for a fixed finite element mesh, and two different error measures: mean (15) **and maximum** (16) **errors. Incoming wave angle is** $\theta = 220^\circ$ **(left) and** $\theta = 310^\circ$ **(right).**

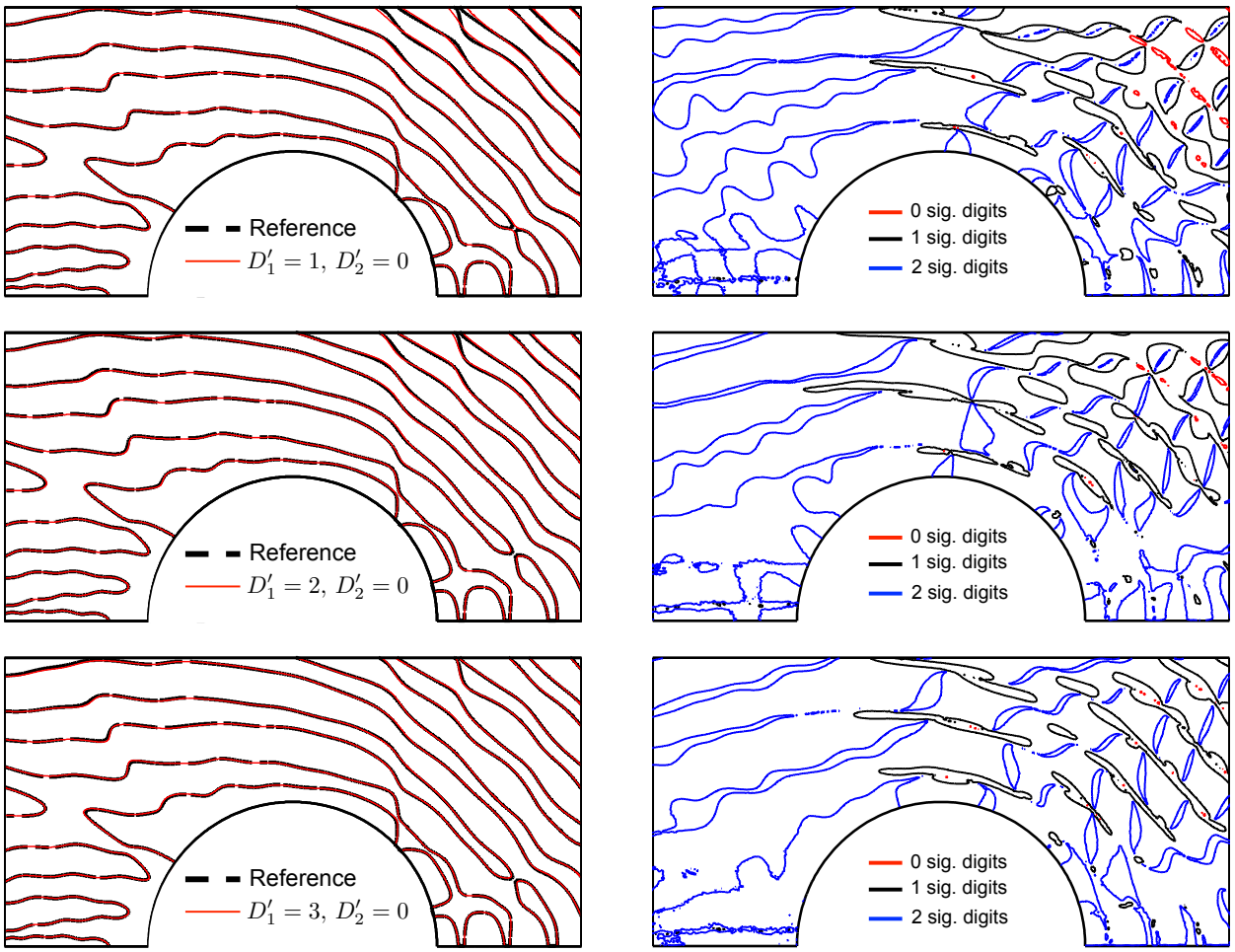

FIG. 7. Semicircular scattering with variable bathymetry: isolines for an amplification factor $H = 1$ (left column) and their corresponding isolines of correct significant digits of accuracy (right column). They are depicted in the interior area of interest defined by $D_1' = D_2' = 0$ for different positions of the left and right PML artificial layers. That is, each row shows the solution and the accuracy provided by a relative distance to PML of $D_1' = 1$ (top row), $D_1' = 2$ (middle row) and $D_1' = 3$ (bottom row). In all cases $D_2' = 0$.

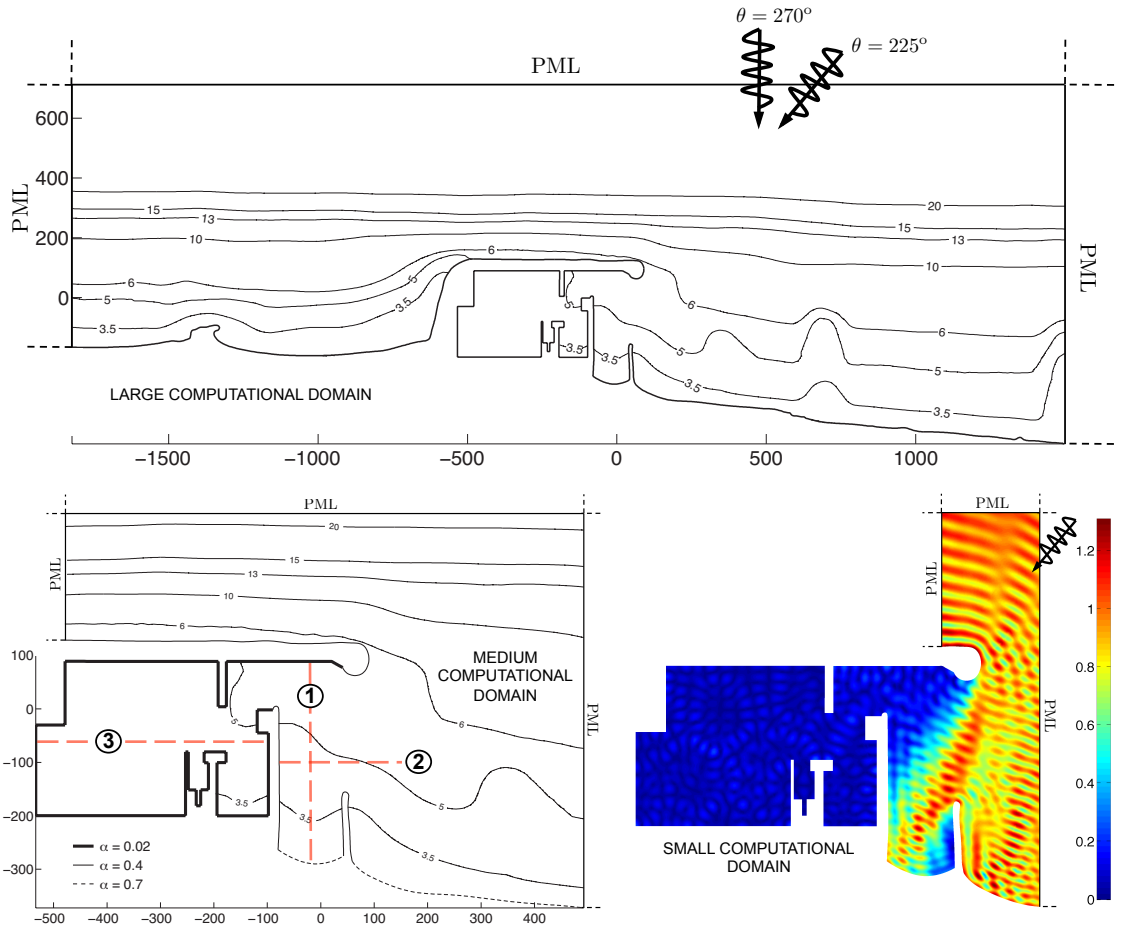

FIG. 8. Mataró harbor: problem statement. Three different computational domains are depicted: largest domain (top), medium domain (bottom left) and small domain (bottom right). Sections 1-3 of interest are highlighted in the domain 1, as well as the absorbing coefficient α in Eq. (3). The solution of the amplification factor for an incoming wave direction of 225° and 6 s of period is shown in the domain 2.

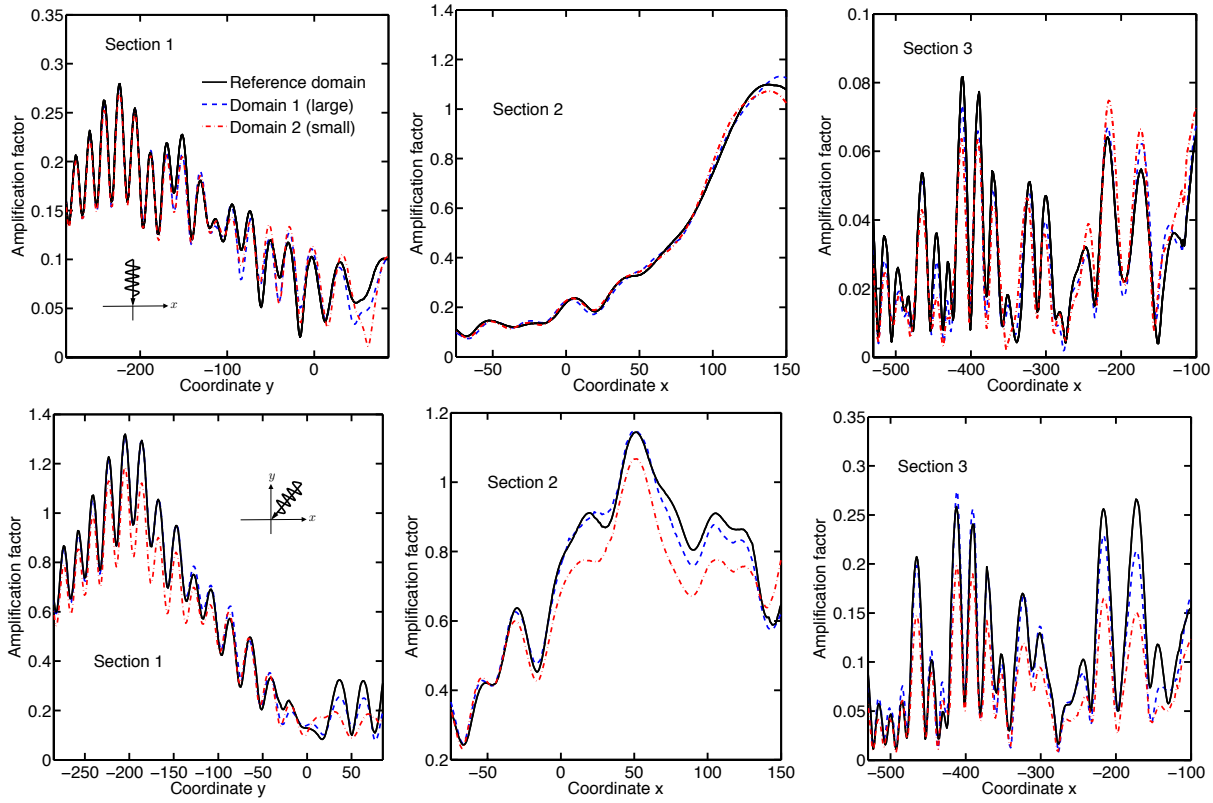

FIG. 9. Mataró harbor: comparison of the amplification factor on the sections of interest for short waves (6 s of period). The incoming wave directions are 270° (top row) and 225° (bottom row).

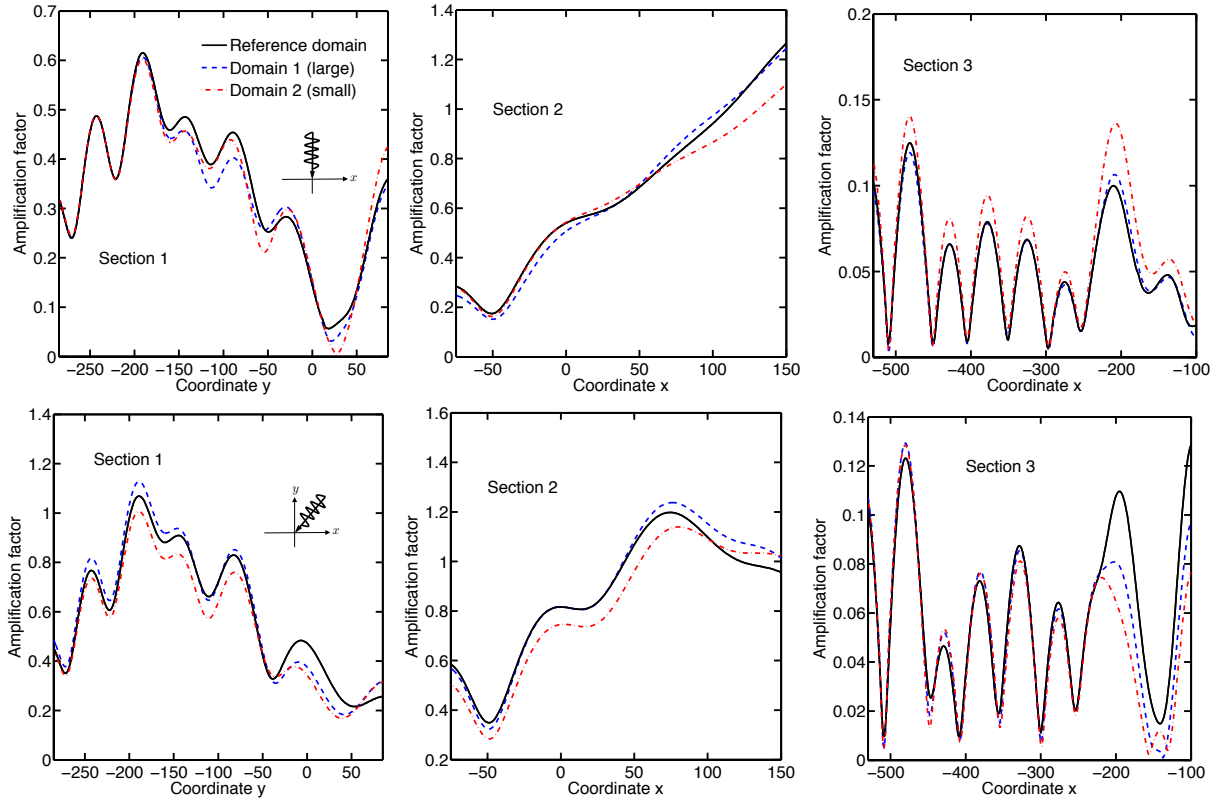

FIG. 10. Mataró harbor: comparison of the amplification factor on the sections of interest for long waves (16 s of period). The incoming wave directions are 270° (top row) and 225° (bottom row).

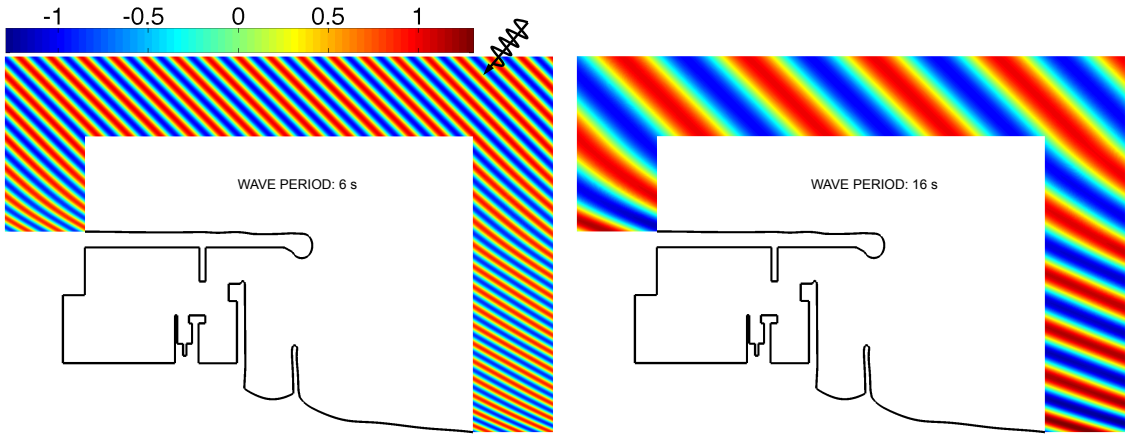

FIG. 11. Mataró harbor with the medium computational domain: the incident wave field is shown for an incoming direction of 225° for short (left) and longer waves (right).